Paper IV:
Blob interactions in 2D scrape-off layer simulations

G. Decristoforo, F. Militello, T. Nicholas, J. Omotani, C. Marsden, N. Walkden and O. E. Garcia,
Physics of Plasmas **27**, 122301 (2020),
doi:10.1063/5.0021314

Physics of Plasmas

Blob interactions in 2D scrape-off layer simulations

Cite as: Phys. Plasmas **27**, 122301 (2020); https://doi.org/10.1063/5.0021314
Submitted: 10 July 2020 . Accepted: 26 October 2020 . Published Online: 01 December 2020

G. Decristoforo, F. Militello, T. Nicholas, J. Omotani, C. Marsden, N. Walkden, and O. E. Garcia

AIP Publishing

Physics of Plasmas ARTICLE scitation.org/journal/php

Blob interactions in 2D scrape-off layer simulations

Cite as: Phys. Plasmas **27**, 122301 (2020); doi: 10.1063/5.0021314
Submitted: 10 July 2020 · Accepted: 26 October 2020 ·
Published Online: 1 December 2020

G. Decristoforo,[1,a] F. Militello,[2] T. Nicholas,[3] J. Omotani,[2] C. Marsden,[4] N. Walkden,[2] and O. E. Garcia[1]

AFFILIATIONS

[1]Department of Physics and Technology, UiT The Arctic University of Norway, NO-9037 Tromsø, Norway
[2]CCFE, Culham Science Centre, Abingdon OX14 3DB, United Kingdom
[3]York Plasma Institute, Department of Physics, University of York, Heslington, York YO10 5DD, United Kingdom
[4]School of Physics and Astronomy, University of Birmingham, Edgbaston, Edgbaston Park Road, Birmingham B15 2TT, United Kingdom

[a)]Author to whom correspondence should be addressed: gregor.decristoforo@uit.no

ABSTRACT

Interaction of coherent structures known as blobs in the scrape-off layer of magnetically confined plasmas is investigated. Isolated and interacting seeded blobs, as well as full plasma turbulence, are studied by two-dimensional numerical simulations. The features of the blobs (position, size, amplitude) are determined with a blob tracking algorithm, which identifies them as coherent structures with amplitudes above a chosen particle density threshold, and their velocities are compared to a conventional center of mass approach. We find that the theoretical velocity-size scaling dependence for isolated blobs is correctly resolved by the blob tracking method. The benchmarked approach is then extended to a population of interacting plasma blobs with statistically distributed amplitudes, sizes, and initial positions for different levels of blob interaction. We observe a correlation between the level of blob interaction and the number of blobs deviating from size–velocity scaling laws of perfectly isolated blobs. This is found to be caused by the interaction of blobs with the electrostatic potential of one another, leading to higher average blob velocities. We introduce a model specific intermittency parameter, quantifying the degree of blob interaction. For interacting blobs, we estimate the deviation from the picture of perfectly isolated blobs as a function of the intermittency parameter. For full plasma turbulence simulations, we observe a strong correlation between the blob amplitudes, sizes, and velocities estimated by the blob tracking algorithm.

I. INTRODUCTION

In tokamaks and other magnetically confined plasma experiments, particle transport in the plasma edge region is dominated by turbulence-driven coherent structures of high density and temperature called blobs or filaments. This can lead to enhanced erosion of the reactor walls and can contribute to the power loads to divertor targets.[1–5] These structures have been observed in multiple plasma devices in all operation regimes using reciprocating or wall mounted Langmuir probes,[6–12] fast visual cameras,[3–5,13–16] and gas puff imaging.[17–22]

In addition to experimental evidence, theoretical understanding of the underlying physical mechanism of blob propagation has been developed in the last 20 years.[23–26] It is understood that the basic mechanism responsible for the radial transport of blobs arises due to grad-B and curvature drifts leading to a charge polarization in the plasma blob/filament. The resulting electric field gives rise to an $\mathbf{E} \times \mathbf{B}$ drift that propels the blob across the magnetic field. Since detailed physical models increase the analytical complexity significantly, the scientific community relies on numerical simulations of isolated blobs and full turbulence simulations of the scrape-off layer. Numerical simulations in two dimensions[27–36] and three dimensions[37–45] have enhanced the understanding of the underlying mechanisms of blob and filament propagation in the scrape-off layer.

Most of these numerical simulations investigate idealized, isolated blobs modeled as positive amplitude and symmetrical Gaussian perturbations on a constant plasma background. This approach has provided an effective way of investigating the influence of specific physical effects, such as finite Larmor radius effects,[46] electromagnetic effects,[47] or parallel electron dynamics[48] on the blob velocity, coherence, and lifetime. Scaling laws describing the radial blob velocity dependence on its amplitudes and size[29,30,34,35,49] have been developed, and different regimes determined by various physical parameters have been discovered.[50,51]

Despite this progress, understanding how well these scaling laws describe blobs in fully turbulent scenarios where they interact with each other is non-trivial. Previous work has shown that single blobs in

close proximity do interact through the electric potential they generate.[52,53] This analysis was performed on two spatially separated and seeded blobs on a constant plasma background and, therefore, does not address the complexity of a fully turbulent plasma environment. In our work, we expand the investigation by starting from isolated blob simulations and then extending our analysis to decreasingly intermittent systems, until we consider fully turbulent scrape-off layer plasma. The intermittency of such a system is a measure of the degree of blob overlap.[54,55] To bridge these two extremes, we use a stochastic model of multiple randomly seeded blobs where blob amplitudes, sizes, initial positions, and the waiting times between consecutive blobs are randomly sampled from given distribution functions.

In order to track blobs in these intermittent and turbulent environments, we implement a tracking algorithm that provides specific blob parameters such as trajectory, velocity, size, and amplitude over the lifetime of individual blobs. Tracking algorithms using either simple threshold methods, defining every coherent structure above a chosen particle density threshold as a blob, or convolutional neural networks, have been presented and applied on two- and three-dimensional data.[56–58] For our analysis, we choose the threshold method since it provides a simple and consistent definition for blobs in both the isolated and the fully turbulent cases. Since there are several ways of defining a blob, this has the advantage of being able to choose an exact and unbiased definition for blobs instead of using machine learning algorithms that require a test dataset. Note that our implementation of a blob tracking algorithm is only designed for numerical simulations where the time and spatial resolution can be chosen. Applying blob tracking techniques on experimental measurements with high speed imaging data using, for example, a watershed algorithm13 is complicated by the spatial and temporal resolution of the measurement techniques. The watershed algorithm is based on fitting two-dimensional Gaussians to local density maxima in order to extract the position, widths, and amplitudes of the fluctuations.

The structure of this publication is as follows: In Sec. II, we present the equations of the physical model that we use for our further analysis. In Sec. III, we present a detailed description of the implementation of the blob tracking algorithm and discuss all relevant parameters of this method. We apply this algorithm on isolated and seeded blob simulations in Sec. IV and compare the results to a conventional center of mass approach. In Sec. V, we extend this analysis to a model seeding multiple blobs randomly. We start with the case of identical amplitudes and starting positions for different levels of intermittency, extend this analysis to random initial positions, and finally to a model including random blob amplitudes. In all cases, we compare the results to the isolated blob simulations. In Sec. VI, we finally apply the blob tracking algorithm on scrape-off layer turbulence simulations and discuss the results in comparison to the previous approaches. A summary and discussion of our results are given in Sec. VII.

II. PHYSICAL MODEL

For our analysis, we choose a standard two-dimensional (2D), two-field fluid model derived from the Braginskii fluid equations.[59–62] We assume for simplicity a quasi-neutral plasma, negligible electron inertia, isothermal electrons (T_e = constant), and cold ions ($T_i = 0$). Note that these assumptions for the electron and ion temperatures are taken for the sake of simplification, as experimental measurements of scrape-off layer plasmas often show high variations of T_e and $T_i > T_e$.[63–68] Nevertheless, this simplified model still captures the fundamental dynamics of the blobs and is therefore sufficient to study their interaction while keeping the number of free parameters of the model relatively low.

For our simulations, we use a simple slab geometry to model the plasma evolution in the two-dimensional plane perpendicular to the magnetic field, with x and y referring to the radial and the binormal/poloidal directions, respectively. The normalized electron particle continuity equation and vorticity equation are given by[28,31,34,60–62]

$$\frac{\mathrm{d}n}{\mathrm{d}t} + g\left(\frac{\partial n}{\partial y} - n\frac{\partial \phi}{\partial y}\right) = D_\perp \nabla_\perp^2 n + F_n - \sigma(n - n_\mathrm{b})\exp(-\phi), \quad (1)$$

$$\frac{\mathrm{d}\nabla_\perp^2 \phi}{\mathrm{d}t} + \frac{g}{n}\frac{\partial n}{\partial y} = \nu_\perp \nabla_\perp^4 \phi + \sigma[1 - \exp(-\phi)], \quad (2)$$

where n represents the electron plasma density and n_b the electron plasma density background. Moreover, ϕ is the electric potential, g is the effective gravity, i.e., interchange drive from magnetic curvature, F_n is the forcing or plasma source term, and $D_\perp$ and $\nu_\perp$ are the collisional dissipative terms representing particle diffusivity and viscosity, respectively. The parameter σ describes the parallel loss rate of the system. The last term on the right hand side of both the particle continuity and electron drift vorticity equations results from modeling the parallel losses to the material surfaces. The forcing for the turbulence simulations is

$$F_n(x) = \frac{1}{w\sqrt{2\pi}}\exp\left(-\frac{1}{2}\frac{(x-\lambda)^2}{w^2}\right), \quad (3)$$

with w and λ providing the width and location of F_n. The source term represents the cross field transport from the core region, but its magnitude and shape chosen here are arbitrary, although convenient. For seeded blob simulations, F_n represents multiple blobs as

$$F_n(x,y,t) = \sum_{k=1}^{K} A_k \exp\left(-\frac{(x-x_k)^2 + (y-y_k)^2}{2\delta_{\perp k}^2}\right)\Delta(t - t_k), \quad (4)$$

where A_k represents the amplitudes, $\delta_{\perp k}$ the widths, x_k and y_k the initial positions, t_k the arrival time of the blobs, and Δ denotes the Dirac delta function.

In order to self-consistently describe order unity relative fluctuation levels, a term given by $\nabla \ln n \cdot \mathrm{d}\nabla_\perp^2 \phi/\mathrm{d}t$ should be added to the left hand side of Eq. (2). Moreover, the dependence on the electron density should be included in the collisional diffusion terms. However, this makes the numerical simulation code much more computer intensive and the simplified model given by Eqs. (1) and (2) has been used here. Further discussion on this topic, commonly referred to as the Boussinesq approximation, can be found in Ref. 36. Strictly, the presented model is derived to describe small density fluctuations and shows inconsistent blob velocity scaling for large amplitudes compared to a non-Boussinesq model. A discussion of this scaling correction is presented in Ref. 35. However, we do not expect this effect to have a significant influence on the qualitative results presented in this work.

The standard Bohm normalization is used for this model equivalent to that used in Refs. 41, 42, and 60–62 and is not discussed here for the sake of brevity. In addition, the advective derivative is given by $\mathrm{d}/\mathrm{d}t = \partial/\partial t + \mathbf{V}_\mathrm{E} \cdot \nabla_\perp$, where $\mathbf{V}_\mathrm{E} = -\nabla_\perp \phi \times \mathbf{B}/B^2$ is the $E \times B$

drift. We approximate **B** to be constant for the $E \times B$ drift even though the effects of magnetic field curvature are considered in the effective gravity g. A discussion of this approximation can also be found in Ref. 35.

We apply periodic boundary conditions in the y-direction and zero gradient boundary conditions in the radial direction for both the density and vorticity fields. For the plasma potential, we choose fixed boundary conditions at the radial boundaries $\phi(x=0) = \phi(x=L_x) = 0$. These boundary conditions are commonly used for numerical reasons,[28,65] despite strictly speaking not being appropriate for scrape-off layer plasmas. The simulation domain is, however, big enough that the boundary conditions for the potential have no measurable effect on the dynamics.

The numerical model is implemented in the STORM code,[52] which is based on BOUT++.[69,70] The code uses a finite difference scheme in the x-direction and a spectral scheme in the y-direction, and time integration is performed by the PVODE solver.[71] We choose a simulation domain size of $L_x = 150$ and $L_y = 100$ with a resolution of 256×256 grid points for all runs. The coefficients are representative of a medium sized machine with $g = 1.7 \times 10^{-3}$ and $\sigma = 1.8 \times 10^{-4}$. The parameters for the source term are $w = 7$ and $\lambda = 30$. For all presented simulations, the background density is set to $n_b = 1$. For single isolated blob simulations in Sec. IV, we choose $D_\perp = \nu_\perp = 2 \times 10^{-2}$, while for the remaining simulations of Secs. V and VI, we take $D_\perp = \nu_\perp = 5 \times 10^{-3}$. We choose higher diffusion coefficients for isolated blob simulations in Sec. IV since the blob coherence stays higher for higher diffusion coefficients and it is more straightforward to test the blob tracking algorithm.

III. BLOB TRACKING

The blob tracking algorithm is implemented in Python, employing the xarray library.[72] Blobs are identified as positive amplitude fluctuations above a certain particle density threshold. The optimal choice of the thresholding technique depends on the problem at hand, and in the case of the isolated blob simulations presented in Sec. IV, we take a constant threshold n_{const} across the whole domain as the blob threshold n_{BT}. For Secs. V–VI, however, we add the binormal/poloidal- and time averaged profile to n_{const}, which takes the form,

$$n_{\text{BT}}(x) = n_{\text{const}} + \frac{1}{L_y\,(T - t_{\text{tr}})} \int_0^{L_y} \mathrm{d}y \int_{t_{\text{tr}}}^{T} \mathrm{d}t\,[n(x,y,t) - n_b], \quad (5)$$

where T stands for the run time of the simulation and t_{tr} for the transient time before the simulation reaches a quasi-stationary state. This method is more robust for turbulence simulations due to the radially varying time-averaged profile.

We label the resulting coherent regions using the multi-dimensional image processing library `scipy.ndimage`. The output data of our simulations is stored as an `xarray` dataset where the simulation variables n, ϕ and the vorticity $\nabla_\perp^2 \phi$ are stored as a three-dimensional array, two dimensions for the spatial coordinates and one dimension for time. We then define a field with the same dimensionality as n with the value one in the regions where n exceeds n_{BT} and zero otherwise. Applying the function `scipy.ndimage.label` on this array returns a field where all coherent regions of ones are labeled from one to the maximum number of coherent structures in the data. We use this field of labels as the definition of blobs in the datasets.

Note that this implementation requires a relatively high temporal resolution of the output files since a blob is only labeled as one coherent structure over time if the blob spatially overlaps with itself in the next frame. The downside of this approach is the resulting large output files, which slows down the memory bound blob tracking algorithm. In addition, one has to consider the periodic boundary condition in the y-direction since the algorithm will label a blob traveling through the y-boundary of the domain as two different objects. For turbulence simulations in Sec. VI, the blob tracking algorithm is only applied in the domain region where $x > 0.4\,L_x$ since we do not include the plasma source region in our analysis.

In order to determine the position and the velocity of the labeled blobs, we determine the center of mass of the blobs at each time step. For isolated blob simulations, the x-component of the center of mass is defined as

$$X_{\text{COM}}(t) = \frac{\int_0^{L_y} \mathrm{d}y \int_0^{L_x} \mathrm{d}x\, x\,[n(x,y,t) - n_b]}{\int_0^{L_y} \mathrm{d}y \int_0^{L_x} \mathrm{d}x [n(x,y,t) - n_b]}, \quad (6)$$

with the y-component defined analogously. For multiply seeded blobs and turbulence simulations, the blob tracking algorithm determines the x-component of the blob position by calculating the center of mass of the plasma region where the plasma density exceeds the threshold, which takes the form

$$X_{\text{BT}}(t) = \frac{\iint_{S_{\text{blob}}} \mathrm{d}x\,\mathrm{d}y\, x\,[n(x,y,t) - n_b]}{\iint_{S_{\text{blob}}} \mathrm{d}x\,\mathrm{d}y [n(x,y,t) - n_b]}, \quad (7)$$

where S_{blob} represents the region where the blob is detected. The algorithm determines the velocity by a finite difference scheme in time and requires therefore the blob being detected for at least two consecutive frames. If a structure is only detected for a single frame, the algorithm sets the velocity to zero. We estimate the blob size δ for each time step as

$$\delta = \left(\frac{1}{\pi} \iint_{S_{\text{blob}}} \mathrm{d}x\,\mathrm{d}y \right)^{1/2}. \quad (8)$$

Note that this definition is based on the assumption that the blob is circular so that $S_{\text{blob}} = \delta^2 \pi$. We choose this definition since it provides a consistent way to compare the detected sizes to seeded circular blobs even though the shape of blobs changes significantly over time. Since this estimate of the blob size varies from the input parameter for the width of seeded blobs $\delta_\perp$, we distinguish between these two variables by dropping the perpendicular-sign for the size estimation from the blob tracking algorithm. Due to this definition, we observe a systematic mismatch between δ and $\delta_\perp$ when estimating the size of a seeded blob with our implementation of the algorithm. We further estimate the peak amplitude A of each blob as

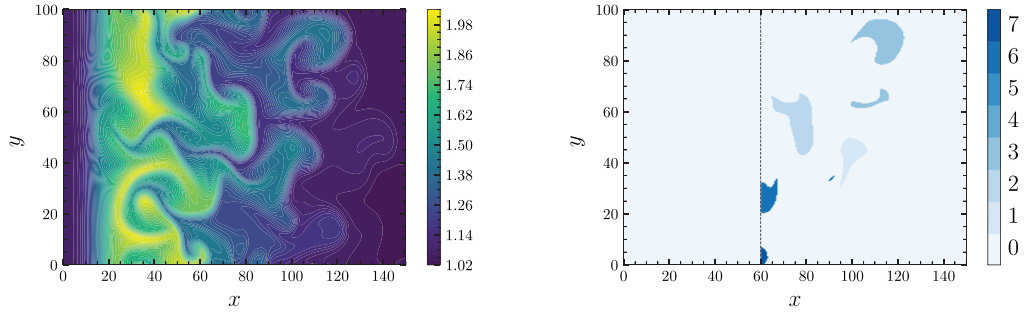

FIG. 1. Snapshots of plasma density n and associated blob labels of a turbulence simulation with parameters equivalent to Sec. II. Here, x refers to the radial and y to the poloidal/binormal coordinate. The colorbar on the right represents the labels of individual detected blobs with the label zero describing the background. The source region on the left side of the domain is excluded from the blob detection algorithm.

$$A = \max_{S_{\text{blob}}}(n(x,y,t) - n_{\text{b}}) \tag{9}$$

for each time step. We will use the here defined blob parameters for our statistical analysis for different forcings. We can then apply this method with the identical blob tracking parameters on isolated blobs, statistically seeded blobs and full scrape-off layer turbulence simulations in order to investigate how blob interaction is affected by the plasma intermittency, and its effect on the blob parameters.

An example of the blob tracking and labeling methods applied on a turbulence simulation is shown in Fig. 1. This figure shows the plasma density and the associated blobs detected by our algorithm. The background is labeled as zero and the individual blobs with ascending numbers.

IV. ISOLATED SEEDED BLOB SIMULATIONS

We begin the analysis by tracking single isolated blobs, seeded on a constant plasma background. We initialize the simulation with a symmetric Gaussian function as a blob as

$$n(x,y,t=0) = n_{\text{b}} + A_0 \exp\left(-\frac{(x-x_0)^2 + (y-y_0)^2}{2\delta_\perp^2}\right), \tag{10}$$

where n_{b} represents the background density, A_0 the initial amplitude, $\delta_\perp$ the initial width, and x_0 and y_0 the initial position of the blob. We choose $x_0 = 0.25\,L_x$ and $y_0 = 0.5\,L_y$. The blob amplitude is set to be as large as the plasma background n_{b}, in this case $A_0 = n_{\text{b}} = 1$. We investigate how the blob velocity evolves over time by estimating the velocity with the blob tracking algorithm for three different thresholds. The results of this analysis are shown in Fig. 2 for a relatively small blob width of $\delta_\perp = 5$. The radial velocity is also determined by a conventional center of mass approach shown in Eq. (6).

The velocity estimates from the algorithm are strongly dependent on the threshold applied for the tracking. For a blob threshold of only one percent of its initial amplitude, we observe that the measured velocity remains very close to the center of mass approach for all widths investigated. This is not surprising since these two implementations are almost identical for low tracking thresholds. For higher blob thresholds, it is shown that the determined maximum radial velocity increases significantly, as the measured radial velocity for a threshold of 40% of the initial blob amplitude more than doubles the center of mass results. This can be explained by the fact that for high thresholds, the algorithm only detects the densest parts of the blob that tends to propagate faster radially than their less dense regions. This has to be taken into account for further work when applying the blob tracking algorithm on more complex models than singular seeded blob simulations. In addition, it is shown that the detected lifetime of the blob for a higher threshold is lower. This can be simply explained by the fact that a narrower detected structure dissipates faster and its amplitude therefore falls below the threshold of the tracking algorithm. The precision of the blob tracking measurement also decreases with higher blob thresholds and smaller blobs. Intuitively, the blob tracking algorithm shows the best performance for wide blobs and low blob thresholds.

We further perform a parameter scan from $\delta_\perp = 2$ to $\delta_\perp = 30$ for the blob width. The results of this analysis are shown in Fig. 3. For all different methods of velocity measurements, we see that the size–velocity dependence follows the analytical predictions derived in previous work.[11,34] The radial velocity of small blobs, which are in the

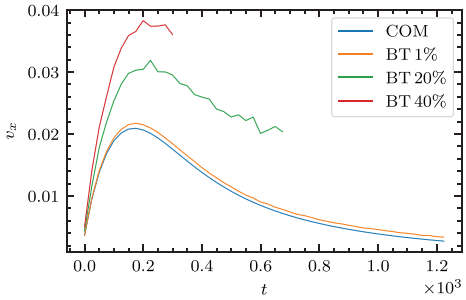

FIG. 2. Radial velocity of an isolated seeded blob width $\delta_\perp = 5$. The blue line refers to the center of mass approach. The other lines refer to the blob tracking algorithm using different percentages of its initial amplitude as the threshold. The radial velocity and the blob width are expressed in normalized units.

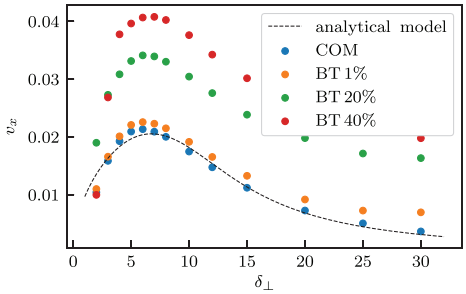

FIG. 3. The dependence of the maximum radial velocity of isolated seeded blobs on their widths compared to an analytical model. The blue dots refer to the center of mass approach, while the other dot colors correspond to the blob tracking algorithm that uses different percentages of the initial amplitude of the blob as a threshold.

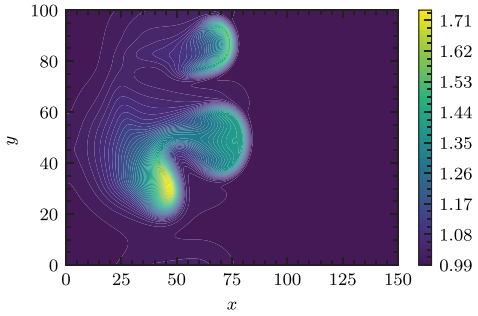

FIG. 4. Snapshot of plasma density n of a simulation of randomly seeded blobs with different amplitudes. The blob at approximately $y = 90$ propagates radially outward almost without interfering with other blobs. At approximately $y = 40$, we see two blobs merging into one coherent structure.

so-called inertial limit, increases with the square root of its size. For large blobs, sheath currents dominate over polarization currents and the blob velocity is inversely proportional to the square of its size. These two limits are referred to as the inertial and sheath connected regimes, respectively.

For all applied blob thresholds, we observe that the scaling dependence is correctly resolved as is the case with the center of mass approach. We therefore conclude that these methods are consistent, which motivates extending our analysis to more complex forcings with multiple seeded blobs.

V. RANDOMLY SEEDED BLOB SIMULATIONS

The next step of our studies is a more complex model, in which blobs are seeded with random parameters, in particular, amplitude A_0, width $\delta_\perp$, initial poloidal/binormal launch positions x_0 and y_0, and waiting time τ_w between the launch of consecutive blobs. This model is still artificial but provides valuable insight in blob interaction in a controlled environment. We start our analysis by only keeping waiting times and widths as random variables and then gradually adding the remaining free parameters to the model. In the most complex case, we sample the waiting times from an exponential distribution of the form,

$$P_{\tau_w} = \frac{1}{\langle \tau_w \rangle} \exp\left(-\frac{\tau_w}{\langle \tau_w \rangle}\right), \tag{11}$$

amplitudes from a truncated exponential distribution and the initial poloidal/binormal starting positions and the widths from a uniform distribution. Note that we choose a uniform distribution for the widths for illustration. Since we intend to compare the velocity-size dependency of detected blobs in this model to isolated blob studies, we choose to sample from a uniform distribution for the sizes to increase the number of large blobs. A snapshot of an example run of this model is presented in Fig. 4 showing the density field of three seeded blobs with different widths and amplitudes. The blob at approximately $y = 90$ propagates in an almost isolated way radially outward. The two blobs at approximately $y = 50$ show a strong interaction with each other and merge eventually into one coherent structure. A less intermittent case with numerous blobs is shown in Fig. 5 where individual blobs interact strongly with each other, resulting in a turbulence-like density snapshot.

In the following analysis, we choose the same parameters for our blob tracking algorithm for all runs, in order to keep comparisons between different models consistent. In order to identify all structures present, one would choose a relatively low threshold for the blob tracking algorithm. Nevertheless, the threshold cannot be set too low in this model that simulates more than one blob since it would label several independent but spatially close structures as one blob. We subtract the time and y-averaged radial profile from the density and apply a blob threshold of 0.2 density units for the resulting fields. In addition, we rerun the blob tracking analysis on single isolated blobs from Sec. IV with these exact parameters to compare these two systems.

A. Single launch-point

We begin our analysis on randomly seeded blobs, keeping the blob amplitudes constant to $A_0 = 1$ and launching all blobs at $x_0 = 0.25\,L_x$ and $y_0 = 0.5\,L_y$, which leaves the waiting times and blob

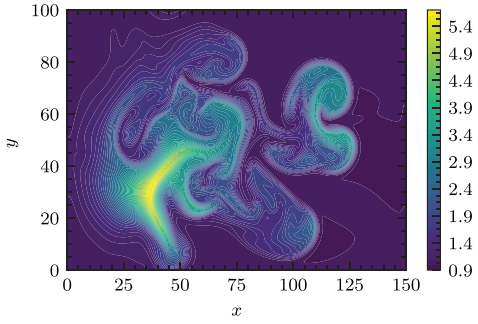

FIG. 5. Snapshot of plasma density n of a simulation of randomly seeded blobs with different amplitudes and low intermittency parameter. We observe strong interactions between individual seeded blobs similar to turbulence simulations.

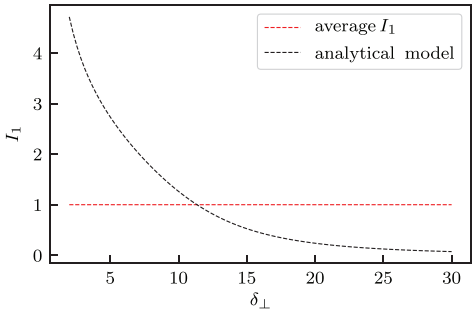

FIG. 6. Model specific intermittency parameter dependence on blob width and with fixed τ_w illustrated utilizing an analytical model for the radial velocity. This is compared to the average intermittency parameter for all $\delta_\perp$.

widths as random variables. In order to quantify the interaction and overlap of individual blobs, we define a model specific intermittency parameter in the spirit of Ref. 54 as

$$I_1 = \frac{\langle v_x \rangle \langle \tau_w \rangle}{\langle \delta \rangle}, \tag{12}$$

where $\langle v_x \rangle$ represents the average radial velocity, $\langle \tau_w \rangle$ the average waiting time, and $\langle \delta \rangle$ the average width of a specific run. This model specific intermittency parameter is introduced in the spirit of previous work on stochastic modeling of intermittent fluctuations, analyzing time series,[68,73–76] which defines the intermittency parameter as the ratio of the average duration time of one event above a chosen threshold and the average waiting time between two such consecutive events. From the definition I_1 is, strictly speaking, not constant but a function of δ of each individual blob. This effect is illustrated in Fig. 6, showing how the blob specific intermittency parameter deviates from the average value. Here, we calculate I_1 for constant $\langle \tau_w \rangle$ where $\langle v_x \rangle$ is given by the analytical solution for $v_x(\delta_\perp)$ in Ref. 34. This has to be taken into consideration for the following investigation. Note that for the presented cases, we calculate $\langle v_x \rangle$ and $\langle \delta \rangle$ not from input parameters of the model but from the blob tracking of seeded blobs excluding structures that only are detected for one frame. We launch blobs for three different average waiting times, which refer to three different states of intermittency. The results of the blob tracking algorithm for these three cases are presented in Fig. 7.

For the most intermittent case of $I_1 = 11.8$, where blobs are the most spatially separated, we see that the overwhelming majority of detected structures have parameters corresponding to isolated blobs. This implies that there is weak interaction between individual blobs. Some individually detected structures show a higher radial velocity than their isolated counterparts. This effect arises due to two closely separated blobs interacting with each other's electrostatic potential. Although this has been studied in some detail in previous work,[52] we deliver an illustration of the physical mechanism in Fig. 8. We seed two identical blobs at different radial positions and apply the blob tracking algorithm to determine their radial velocity. The electrostatic potential created by the two separate blobs superposes and results in a stronger electric field, which increases the $\mathbf{E} \times \mathbf{B}$ drift that pulls the coherent blob structures radially outward. This effect can lead to the formation of so-called "blob trenches" in turbulence simulations. We estimate the radial velocity of the two blobs with the blob tracking algorithm and observe a clear increase in velocity for the trailing blob, shown in Fig. 9. The case of two blobs in the poloidal/binormal direction is also studied in Ref. 52, showing a decrease in the radial velocity compared to the isolated case. However, blobs in turbulent environments usually get diverted into the blob trenches by the electrostatic potential of previous blobs. We, therefore, observe significantly more cases of blobs in close radial than in poloidal/binormal proximity.

For $I_1 = 4.9$ and $I_1 = 1.8$ in Fig. 7, we observe an increasing number of blobs with a higher radial velocity than their isolated counterparts. Since the average waiting time decreases, individual blobs interact strongly through the potentials of nearby blobs and get accelerated radially outward. In addition, the blob tracking algorithm detects more smaller-sized coherent structures that usually have short lifetimes, often only one to two frames. Due to the increasing interactions and turbulent flow in this model, more of these small structures are detected by the algorithm, which can be classed as numerical artifacts.

B. Random launch-point

The next random variable of the investigated model added to our analysis is the poloidal/binormal launch position of the seeded blobs. We sample the launch position y_k from a uniform distribution $U(0.2\,L_y, 0.8\,L_y)$ to reduce the number of blobs propagating through the poloidal/binormal boundaries. The initial amplitudes remain a fixed parameter set to $A_0 = 1$. Seeding blobs from a random poloidal/

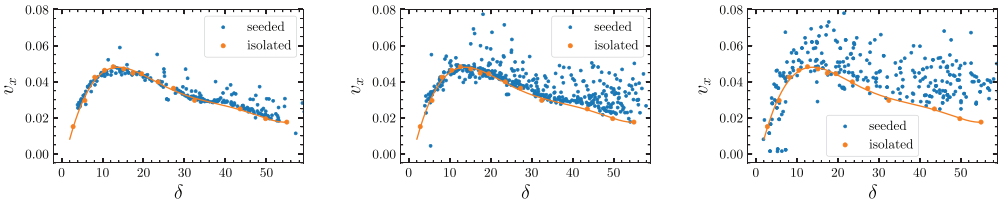

FIG. 7. Maximum radial velocity measured with the tracking algorithm of randomly seeded blobs with single launch position (blue dots) compared to isolated blobs (orange dots). The intermittency parameters for the displayed runs are approximately $I = 11.8$ (left), $I = 4.9$ (middle), and $I = 1.8$ (right). Blob widths are sampled from a uniform distribution with $\delta_\perp \in U(2, 30)$ and waiting times from an exponential distribution. The average waiting times for the displayed runs are $\langle \tau_w \rangle = 200$ (left), $\langle \tau_w \rangle = 75$ (middle), and $\langle \tau_w \rangle = 25$ (right).

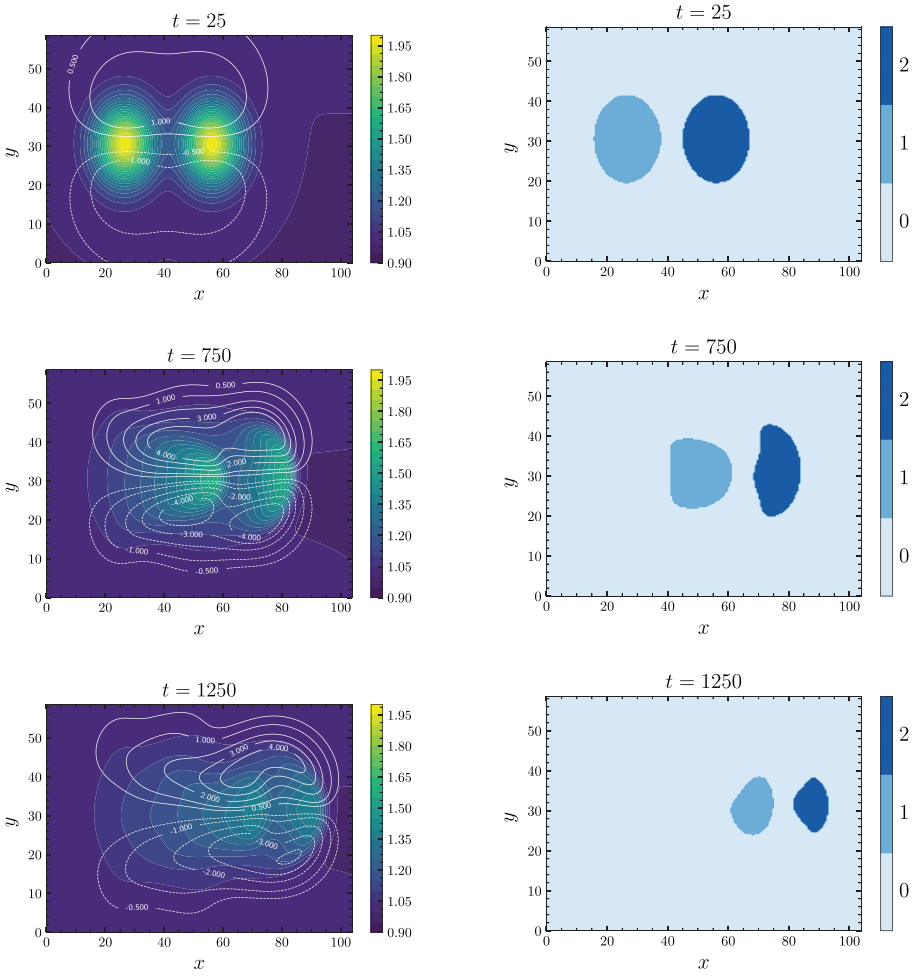

FIG. 8. Snapshot of the plasma density of two seeded identical blobs with their electrostatic potential indicated with white lines (left) and the associated blob labels, detected by the blob tracking algorithm at three different time steps (right). The label zero describes the background particle density. The interaction of the trailing blob by the electrostatic potential of the leading blob is illustrated.

binormal position increases the intermittency of the model and leads to more complex interactions between individual structures. We therefore multiply the expression for the intermittency parameter shown in Eq. (13) with $L_y/3\langle\delta\rangle$ resulting in

$$I_2 = \frac{\langle v_x\rangle\langle\tau_w\rangle L_y}{3\langle\delta\rangle^2} \tag{13}$$

to consider this extension of the model since $L_y/3$ is the average distance of two randomly chosen events from a uniform distribution with length L_y. We run this model for three different intermittency parameters and present the results from the detected blobs in Fig. 10. As one might expect, most detected structures in the $I_2 = 7.6$ case follow the isolated blob line but show more spread around this line than in the single launch point model. In particular, many small blobs are detected by the blob tracking algorithm that show a significantly lower radial velocity than their isolated counterparts, with some blobs even showing a negative radial velocity. We provide an explanation for this effect in Fig. 11. It is shown that these small blobs deviating from the

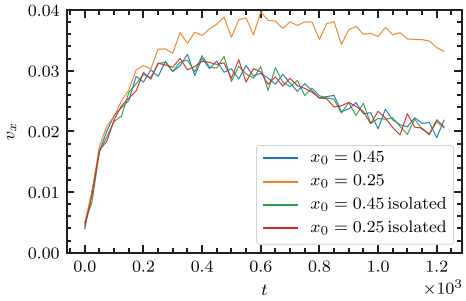

FIG. 9. Radial velocity of two seeded identical blobs at two different radial positions and their isolated counterparts. The Blob, seeded at $x_0 = 0.25$, which is trailing the blob seeded at $x_0 = 0.45$, shows a significant increase in the radial velocity due to the electrostatic potential created by the leading blob.

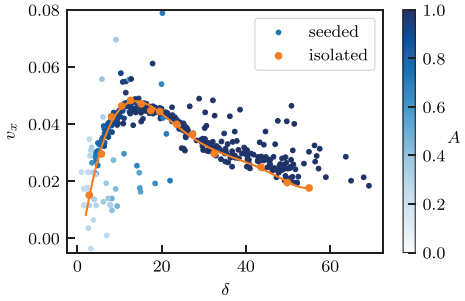

FIG. 11. Radial velocity and widths of detected blobs with an intermittency parameter of $I_2 = 7.6$ are compared to isolated blobs (orange dots). Blobs with a small maximum amplitude represent most small structures deviating from the scaling laws of isolated blobs.

theoretical predictions have a maximum amplitude significantly lower than $A = 1$ as the initially seeded blobs have. This indicates that these small structures result from the complex interaction of the seeded blobs. Since their amplitudes are significantly lower than the ones of their isolated counterparts, their radial velocity is also lower. For the cases of lower intermittency parameters, we observe again an increase in the average radial velocities and the spread. This remains consistent with the previous single launch point model and can be explained by the same blob-interaction mechanism.

We utilize the presented six runs to quantify the interaction of individual blobs for different intermittency parameters. For each model, we calculate the average deviation in radial velocity of the detected structures from the fit function of the isolated blobs. The result is shown in Fig. 12. The six data points are compared to a fit of the inverse of I times a constant. This clearly suggests that the intermittency of blobs in the scrape-off layer has a strong effect on their radial velocity and propagation.

C. Amplitude distribution

We add the final random variable of our model by seeding blobs with truncated exponentially distributed amplitudes since we only choose amplitudes with $0.5 < A_0 < 3$ in order to compare them more easily with isolated seeded blobs. We perform a parameter scan for blob widths for isolated seeded blobs with amplitudes $A_0 = 0.5$ and $A_0 = 3$ in order to create reference values for the boundaries of our model. We then run our model for three different intermittency parameters and compare the results with the isolated blobs for different amplitudes. These results are shown in Fig. 13.

The results are consistent with our previous analysis. Most randomly seeded blobs lie in between the borders established by the isolated blobs. For small blobs, we observe again some data points with a lower radial velocity than in the isolated case, which can be explained by the same effect as in Sec. V B. For wider structures, we find some structures with higher velocities, which can again be explained by the electrostatic potential of interacting blobs. As expected, the average velocity is increasing for a decreasing intermittency parameter.

VI. TURBULENCE SIMULATIONS

After investigating randomly seeded blob models, we turn our attention to a simple self-consistent scrape-off layer model simulating plasma turbulence. Numerically, the model is equivalent to the seeded blob simulations but uses the term of Eq. (3) as a plasma source instead of Gaussian seeded blobs. The density profile in the simulation domain is built and balanced by the plasma source and the sheath dissipation included in the model. These are unstable due to bad curvature and interchange instability, which leads to coherent structures of plasma propagating outward radially due to the blob mechanism

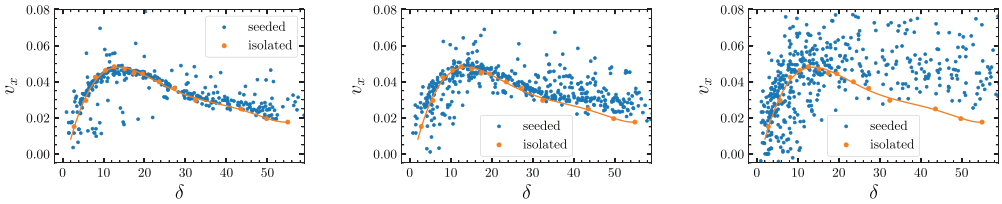

FIG. 10. Maximum radial velocity measured with the tracking algorithm of randomly seeded blobs with the random poloidal/binormal launch position (blue dots) compared to isolated blobs (orange dots). The intermittency parameters for the displayed runs are approximately $I_2 = 7.6$ (left), $I_2 = 2.5$ (middle), and $I_2 = 1.3$ (right). Widths are sampled from $\delta_\perp \in U(2, 30)$, initial poloidal/binormal positions from $y_0 \in U(0.2 \times L_y, 0.8 \times L_y)$, and waiting times from an exponential distribution. The average waiting times for the displayed runs are $\langle \tau_w \rangle = 120$ (left), $\langle \tau_w \rangle = 50$ (middle), and $\langle \tau_w \rangle = 13$ (right).

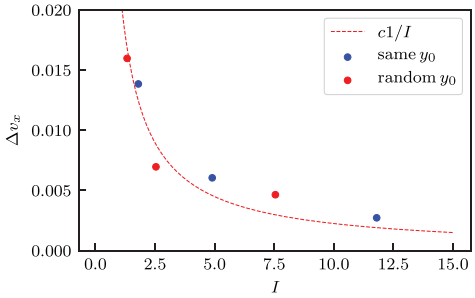

FIG. 12. Average deviation in the radial velocity of theoretical scaling law predictions measured in randomly seeded blob simulations for different intermittency parameters. The relationship between Δv_x and I is compared to a fit of the inverse of I times a constant.

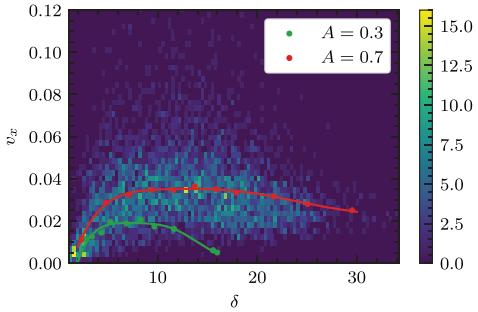

FIG. 14. Radial velocity of blobs detected in full turbulence simulations compared to isolated blobs with $A = 0.3$ and $A = 0.7$. Blobs only detected for one frame are excluded, as well as blobs close to the poloidal/binormal simulation boundary.

discussed in Sec. I. These blob like structures vary in amplitude and width and can be detected and tracked by the tracking algorithm.

We exclude the source region for our blob tracking analysis and only consider coherent structures detected at $x > 0.4\,L_x$ since this unphysical term only serves as a numerical term. In addition, we only include blobs with an initial center of mass of $0.25\,L_y < y_{\text{init}} < 0.75\,L_y$ in our statistical evaluation in order to exclude distorted tracked structures because of the periodic boundary conditions in the y-dimension. Even though it is straightforward to track blobs consistently that traverse the simulation border in this direction, our numerical implementation for this issue is computationally more expensive than running the simulation longer and only considering blobs in the central band of the domain. For such turbulence simulations, the tracking algorithm identifies numerous small structures that only appear for one frame. These structures represent approximately one third of the total number of detected blobs and are also excluded from our statistical analysis. The remaining parameters for the tracking algorithm stay the same as for the randomly seeded blob model. The determined radial velocities and sizes of the detected blobs in the turbulence simulation are shown as a 2D histogram in Fig. 14. We choose this type of plot since the illustrated 4542 blobs are too many to be shown distinctively in a scatterplot. The distribution of the sizes and amplitudes of the detected structures, as well as the joint probability distribution functions (PDFs) of these two blob parameters, are shown in Fig. 15.

These measurements show that the amplitudes lie in between $A = 0.2$, which is equivalent to the threshold used for the blob tracking algorithm, and $A = 0.7$. Since blobs with an amplitude smaller than $A = 0.2$ are not detected and since many small blobs below $A = 0.4$ are dissipated too quickly to be detected, the shown PDF is not representative for all structures in the system. Taking these factors into account, the common assumption of blob amplitudes being exponentially distributed cannot be falsified by these measurements. The same is valid for the distribution of blob widths. Nevertheless, we observe a clear correlation between the amplitudes and widths as the correlation coefficient of these two parameters is $\rho = 0.85$. In order to compare the detected blobs with their isolated counterparts, we perform a parameter scan for blobs with the amplitudes $A_0 = 0.7$ and $A_0 = 0.3$ as the two edge values of the distribution. Since $A_0 = 0.2$ would be too small to be detected by the algorithm, we use $A_0 = 0.3$ as the lower border. These isolated blobs are shown together with their fit in Fig. 14. In this analysis, no blobs with a higher width than $\delta = 30$ appear; therefore, we rarely observe the decreasing radial velocity for bigger and denser blobs in our velocity–size scaling. Nevertheless, the dataset provides enough information to discuss the results in comparison to isolated blob simulations. As in the previous model of randomly seeded blobs with random amplitudes, we observe that the overwhelming majority

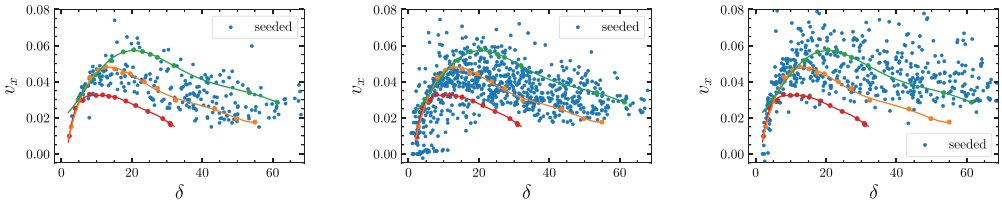

FIG. 13. Maximum radial velocity measured with the tracking algorithm of randomly seeded blobs with the random poloidal launch position and truncated exponentially distributed amplitudes (blue dots) compared to isolated blobs with $A_0 = 0.5$ (red dots), $A_0 = 1$ (orange dots), and $A_0 = 3$ (green dots). The intermittency parameters for the displayed runs are approximately $I = 10.3$ (left), $I = 7.9$ (middle), and $I = 1.7$ (right). The average waiting times for the displayed runs are $\langle \tau_w \rangle = 200$ (left), $\langle \tau_w \rangle = 75$ (middle), and $\langle \tau_w \rangle = 25$ (right).

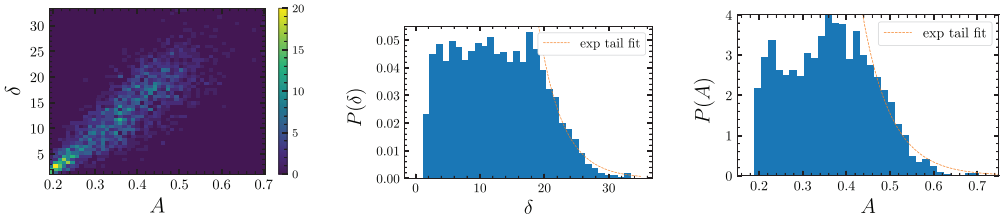

FIG. 15. 2D histogram showing the correlation of the maximum amplitudes and widths (left) resulting in a correlation coefficient of $\rho = 0.85$. Probability density functions of maximum width (middle) and amplitudes (right) of detected blobs in a fully turbulent simulation. The tail of the PDFs is compared to an exponential fit.

of detected blob structures lie in between the trends of the isolated blob simulations. As for the previous model, the algorithm detects a significant number of structures with a higher radial velocity than the isolated blobs. We explain these events again by the interaction of blobs with the electrostatic potential of one another. Due to these findings, we conclude that tracking blobs in a fully turbulent scenario shows very similar results to models of statistically seeded blobs. While the theoretical size–velocity scaling of isolated blobs gives a reasonable order of magnitude estimate, there is an order unity scatter due to strong interactions between blobs.

VII. DISCUSSION AND CONCLUSION

In this work, we investigated the interaction of blobs in the scrape-off layer for different models of varying complexity. In particular, we compared the relation between the radial velocity and the widths of the blobs with established scaling laws. We started with studying isolated blobs and extended our analysis on a model of randomly seeded blobs where the parameters are sampled from physically adequate PDFs. We studied this model for different levels of intermittency and applied the acquired knowledge on fully turbulent scrape-off layer plasma simulations.

In this process, we developed a blob tracking algorithm as a versatile tool to analyze and understand blob and plasma parameters in scrape-off layer plasma simulations. We publish our implementation on github under https://github.com/gregordecristoforo/xblobs. The current version of the algorithm can be applied on any 2D `xarray` dataset with a cartesian grid and constant spacing `dx`, `dy` and `dt`.[77] An extension of the algorithm to three dimensions is numerically easy to implement, but the 2D version of this algorithm can be valuable for analyzing blob propagation and turbulent transport, in a specific plane in three-dimensional plasma simulations. We will use this in the future to study how blob properties depend on specific physical effects or study the plasma transport in the scrape-off layer.

For isolated blob simulations, we find that the velocity-size scaling dependence is correctly resolved by the blob tracking method. For the case of non-isolated blobs, we observe a correlation between the level of blob interaction and the number of blobs deviating from size–velocity scaling laws of perfectly isolated blobs. Blobs show an increase in the radial velocity in cases of low intermittency for the randomly seeded blob model and turbulence model, compared to isolated and intermittent cases. We explain this observation by the interaction of blobs with the electrostatic potential of one another. The blob trajectories are influenced by the electrostatic potential, which gets diverted, leading to the creation of trenches in which blobs get accelerated by the potential of ones in front of them. These findings are consistent with previous work studying the interaction of two seeded blobs.[52] Additionally, we find a strong correlation between the blob amplitudes and sizes estimated by the blob tracking algorithm for full plasma turbulence simulations. For all studied forcings, we observe a systematical size–velocity relationship consistent with theoretical predictions from the model. This concludes that despite the significant interaction of blobs, they still follow established scaling laws and can therefore be regarded to the lowest order, as isolated structures propagating radially through the scrape-off layer. We thereby display the relevance of isolated seeded blob and filament simulations for complex turbulent models.

ACKNOWLEDGMENTS

This work was supported by the UiT Aurora Centre Program, UiT The Arctic University of Norway (2020). G.D. acknowledges the generous hospitality of the Culham Centre for Fusion Energy (CCFE) where this work was conducted. In addition, this work has been partially funded by the EPSRC Grant No. EP/T012250/1 and partially carried out within the framework of the EUROfusion Consortium and has received funding from the Euratom research and training programmes 2014–2018 and 2019–2020 under Grant Agreement No. 633053. The views and opinions expressed herein do not necessarily reflect those of the European Commission. The MARCONI supercomputer was used for parts of the computational work under the Project No. FUA34_SOLBOUT4.

DATA AVAILABILITY

The data that support the findings of this study are available from the corresponding author upon reasonable request.

REFERENCES

[1]G. Antar, S. Krasheninnikov, P. Devynck, R. Doerner, E. Hollmann, J. Boedo, S. Luckhardt, and R. Conn, "Experimental evidence of intermittent convection in the edge of magnetic confinement devices," Phys. Rev. Lett. **87**, 065001 (2001).
[2]G. Y. Antar, G. Counsell, Y. Yu, B. LaBombard, and P. Devynck, "Universality of intermittent convective transport in the scrape-off layer of magnetically confined devices," Phys. Plasmas **10**, 419–428 (2003).
[3]A. Kirk, N. B. Ayed, G. Counsell, B. Dudson, T. Eich, A. Herrmann, B. Koch, R. Martin, A. Meakins, S. Saarelma *et al.*, "Filament structures at the plasma edge on MAST," Plasma Phys. Controlled Fusion **48**, B433 (2006).
[4]B. Dudson, N. B. Ayed, A. Kirk, H. Wilson, G. Counsell, X. Xu, M. Umansky, P. Snyder, and B. LLoyd, "Experiments and simulation of edge turbulence and filaments in MAST," Plasma Phys. Controlled Fusion **50**, 124012 (2008).

[5]N. B. Ayed, A. Kirk, B. Dudson, S. Tallents, R. Vann, and H. Wilson, "Inter-ELM filaments and turbulent transport in the mega-amp spherical tokamak," Plasma Phys. Controlled Fusion **51**, 035016 (2009).
[6]J. A. Boedo, D. Rudakov, R. Moyer, S. Krasheninnikov, D. Whyte, G. McKee, G. Tynan, M. Schaffer, P. Stangeby, P. West *et al.*, "Transport by intermittent convection in the boundary of the DIII-D tokamak," Phys. Plasmas **8**, 4826–4833 (2001).
[7]D. Rudakov, J. Boedo, R. Moyer, S. Krasheninnikov, A. Leonard, M. Mahdavi, G. McKee, G. Porter, P. Stangeby, J. Watkins *et al.*, "Fluctuation-driven transport in the DIII-D boundary," Plasma Phys. Controlled Fusion **44**, 717 (2002).
[8]J. A. Boedo, D. L. Rudakov, R. A. Moyer, G. R. McKee, R. J. Colchin, M. J. Schaffer, P. Stangeby, W. West, S. L. Allen, T. E. Evans *et al.*, "Transport by intermittency in the boundary of the DIII-D tokamak," Phys. Plasmas **10**, 1670–1677 (2003).
[9]O. E. Garcia, J. Horacek, R. Pitts, A. H. Nielsen, W. Fundamenski, V. Naulin, and J. J. Rasmussen, "Fluctuations and transport in the TCV scrape-off layer," Nucl. Fusion **47**, 667 (2007).
[10]O. E. Garcia, R. Pitts, J. Horacek, J. Madsen, V. Naulin, A. H. Nielsen, and J. J. Rasmussen, "Collisionality dependent transport in TCV SOL plasmas," Plasma Phys. Controlled Fusion **49**, B47 (2007).
[11]C. Theiler, I. Furno, P. Ricci, A. Fasoli, B. Labit, S. Müller, and G. Plyushchev, "Cross-field motion of plasma blobs in an open magnetic field line configuration," Phys. Rev. Lett. **103**, 065001 (2009).
[12]F. Militello, P. Tamain, W. Fundamenski, A. Kirk, V. Naulin, and A. H. Nielsen, "Experimental and numerical characterization of the turbulence in the scrape-off layer of MAST," Plasma Phys. Controlled Fusion **55**, 025005 (2013).
[13]T. Farley, F. Militello, N. Walkden, J. Harrison, S. Silburn, and J. Bradley, "Analysis of filament statistics in fast camera data on MAST," in APS Meeting Abstracts, 2017.
[14]N. Walkden, J. Harrison, S. Silburn, T. Farley, S. S. Henderson, A. Kirk, F. Militello, and A. Thornton, "Quiescence near the X-point of MAST measured by high speed visible imaging," Nucl. Fusion **57**, 126028 (2017).
[15]N. Walkden, F. Militello, J. Harrison, T. Farley, S. Silburn, and J. Young, "Identification of intermittent transport in the scrape-off layer of MAST through high speed imaging," Nucl. Mater. Energy **12**, 175–180 (2017).
[16]N. Walkden, B. Labit, H. Reimerdes, J. Harrison, T. Farley, P. Innocente, and F. Militello, "Fluctuation characteristics of the TCV snowflake divertor measured with high speed visible imaging," Plasma Phys. Controlled Fusion **60**, 115008 (2018).
[17]S. Zweben, D. Stotler, J. Terry, B. LaBombard, M. Greenwald, M. Muterspaugh, C. Pitcher, A. C. Group, K. Hallatschek, R. Maqueda *et al.*, "Edge turbulence imaging in the alcator C-Mod tokamak," Phys. Plasmas **9**, 1981–1989 (2002).
[18]J. Terry, S. Zweben, K. Hallatschek, B. LaBombard, R. Maqueda, B. Bai, C. Boswell, M. Greenwald, D. Kopon, W. Nevins *et al.*, "Observations of the turbulence in the scrape-off-layer of alcator C-Mod and comparisons with simulation," Phys. Plasmas **10**, 1739–1747 (2003).
[19]J. Myra, D. D'Ippolito, D. Stotler, S. Zweben, B. LeBlanc, J. Menard, R. Maqueda, and J. Boedo, "Blob birth and transport in the tokamak edge plasma: Analysis of imaging data," Phys. Plasmas **13**, 092509 (2006).
[20]O. Grulke, J. Terry, B. LaBombard, and S. Zweben, "Radially propagating fluctuation structures in the scrape-off layer of alcator C-Mod," Phys. Plasmas **13**, 012306 (2006).
[21]S. Zweben, W. Davis, S. Kaye, J. Myra, R. Bell, B. LeBlanc, R. Maqueda, T. Munsat, S. Sabbagh, Y. Sechrest *et al.*, "Edge and SOL turbulence and blob variations over a large database in NSTX," Nucl. Fusion **55**, 093035 (2015).
[22]S. Zweben, J. Myra, W. Davis, D. D'Ippolito, T. Gray, S. Kaye, B. LeBlanc, R. Maqueda, D. Russell, D. Stotler *et al.*, "Blob structure and motion in the edge and SOL of NSTX," Plasma Phys. Controlled Fusion **58**, 044007 (2016).
[23]D. D'Ippolito, J. Myra, S. Krasheninnikov, G. Yu, and A. Y. Pigarov, "Blob transport in the tokamak scrape-off-layer," Contrib. Plasma Phys. **44**, 205–216 (2004).
[24]D. D'Ippolito, J. Myra, and S. Zweben, "Convective transport by intermittent blob-filaments: Comparison of theory and experiment," Phys. Plasmas **18**, 060501 (2011).
[25]S. Krasheninnikov, D. D'Ippolito, and J. Myra, "Recent theoretical progress in understanding coherent structures in edge and sol turbulence," J. Plasma Phys. **74**, 679–717 (2008).
[26]O. E. Garcia, "Blob transport in the plasma edge: A review," Plasma Fusion Res. **4**, 019 (2009).
[27]N. Bian, S. Benkadda, J.-V. Paulsen, and O. E. Garcia, "Blobs and front propagation in the scrape-off layer of magnetic confinement devices," Phys. Plasmas **10**, 671–676 (2003).
[28]O. E. Garcia, V. Naulin, A. Nielsen, and J. J. Rasmussen, "Computations of intermittent transport in scrape-off layer plasmas," Phys. Rev. Lett. **92**, 165003 (2004).
[29]O. E. Garcia, N. Bian, V. Naulin, A. Nielsen, and J. J. Rasmussen, "Mechanism and scaling for convection of isolated structures in nonuniformly magnetized plasmas," Phys. Plasmas **12**, 090701 (2005).
[30]O. E. Garcia, N. Bian, and W. Fundamenski, "Radial interchange motions of plasma filaments," Phys. Plasmas **13**, 082309 (2006).
[31]D. Russell, J. Myra, and D. D'Ippolito, "Saturation mechanisms for edge turbulence," Phys. Plasmas **16**, 122304 (2009).
[32]F. Militello, W. Fundamenski, V. Naulin, and A. H. Nielsen, "Simulations of edge and scrape off layer turbulence in mega ampere spherical tokamak plasmas," Plasma Phys. Controlled Fusion **54**, 095011 (2012).
[33]F. Militello, V. Naulin, and A. H. Nielsen, "Numerical scalings of the decay lengths in the scrape-off layer," Plasma Phys. Controlled Fusion **55**, 074010 (2013).
[34]R. Kube and O. E. Garcia, "Velocity scaling for filament motion in scrape-off layer plasmas," Phys. Plasmas **18**, 102314 (2011).
[35]R. Kube, O. E. Garcia, and M. Wiesenberger, "Amplitude and size scaling for interchange motions of plasma filaments," Phys. Plasmas **23**, 122302 (2016).
[36]M. Wiesenberger, M. Held, R. Kube, and O. E. Garcia, "Unified transport scaling laws for plasma blobs and depletions," Phys. Plasmas **24**, 064502 (2017).
[37]J. R. Angus, M. V. Umansky, and S. I. Krasheninnikov, "Effect of drift waves on plasma blob dynamics," Phys. Rev. Lett. **108**, 215002 (2012).
[38]N. Walkden, B. Dudson, and G. Fishpool, "Characterization of 3D filament dynamics in a MAST SOL flux tube geometry," Plasma Phys. Controlled Fusion **55**, 105005 (2013).
[39]P. Ricci, F. Riva, C. Theiler, A. Fasoli, I. Furno, F. Halpern, and J. Loizu, "Approaching the investigation of plasma turbulence through a rigorous verification and validation procedure: A practical example," Phys. Plasmas **22**, 055704 (2015).
[40]P. Tamain, H. Bufferand, G. Ciraolo, C. Colin, P. Ghendrih, F. Schwander, and E. Serre, "3D properties of edge turbulent transport in full-torus simulations and their impact on poloidal asymmetries," Contrib. Plasma Phys. **54**, 555–559 (2014).
[41]L. Easy, F. Militello, J. Omotani, B. Dudson, E. Havlíčková, P. Tamain, V. Naulin, and A. H. Nielsen, "Three dimensional simulations of plasma filaments in the scrape off layer: A comparison with models of reduced dimensionality," Phys. Plasmas **21**, 122515 (2014).
[42]L. Easy, F. Militello, J. Omotani, N. Walkden, and B. Dudson, "Investigation of the effect of resistivity on scrape off layer filaments using three-dimensional simulations," Phys. Plasmas **23**, 012512 (2016).
[43]F. Militello, N. Walkden, T. Farley, W. Gracias, J. Olsen, F. Riva, L. Easy, N. Fedorczak, I. Lupelli, J. Madsen *et al.*, "Multi-code analysis of scrape-off layer filament dynamics in MAST," Plasma Phys. Controlled Fusion **58**, 105002 (2016).
[44]F. Riva, C. Colin, J. Denis, L. Easy, I. Furno, J. Madsen, F. Militello, V. Naulin, A. H. Nielsen, J. M. B. Olsen *et al.*, "Blob dynamics in the TORPEX experiment: A multi-code validation," Plasma Phys. Controlled Fusion **58**, 044005 (2016).
[45]F. Riva, F. Militello, S. Elmore, J. T. Omotani, B. D. Dudson, and N. Walkden, "Three-dimensional plasma edge turbulence simulations of MAST and comparison with experimental measurements," Plasma Phys. Controlled Fusion **61**, 095013 (2019).
[46]M. Wiesenberger, J. Madsen, and A. Kendl, "Radial convection of finite ion temperature, high amplitude plasma blobs," Phys. Plasmas **21**, 092301 (2014).
[47]W. Lee, J. R. Angus, M. V. Umansky, and S. I. Krasheninnikov, "Electromagnetic effects on plasma blob-filament transport," J. Nucl. Mater. **463**, 765–768 (2015).
[48]J. R. Angus, S. I. Krasheninnikov, and M. V. Umansky, "Effects of parallel electron dynamics on plasma blob transport," Phys. Plasmas **19**, 082312 (2012).

[49]S. I. Krasheninnikov, "On scrape off layer plasma transport," Phys. Lett. A **283**, 368–370 (2001).
[50]J. Myra, D. Russell, and D. D'Ippolito, "Collisionality and magnetic geometry effects on tokamak edge turbulent transport. I. A two-region model with application to blobs," Phys. Plasmas **13**, 112502 (2006).
[51]D. Russell, J. Myra, and D. D'Ippolito, "Collisionality and magnetic geometry effects on tokamak edge turbulent transport. II. Many-blob turbulence in the two-region model," Phys. Plasmas **14**, 102307 (2007).
[52]F. Militello, B. Dudson, L. Easy, A. Kirk, and P. Naylor, "On the interaction of scrape off layer filaments," Plasma Phys. Controlled Fusion **59**, 125013 (2017).
[53]A. Kendl, "Gyrofluid vortex interaction," Plasma Phys. Controlled Fusion **60**, 025017 (2018).
[54]O. E. Garcia, "Stochastic modeling of intermittent scrape-off layer plasma fluctuations," Phys. Rev. Lett. **108**, 265001 (2012).
[55]O. E. Garcia, S. M. Fritzner, R. Kube, I. Cziegler, B. LaBombard, and J. L. Terry, "Intermittent fluctuations in the Alcator C-Mod scrape-off layer," Phys. Plasmas **20**, 055901 (2013).
[56]F. Nespoli, I. Furno, B. Labit, P. Ricci, F. Avino, F. Halpern, F. Musil, and F. Riva, "Blob properties in full-turbulence simulations of the TCV scrape-off layer," Plasma Phys. Controlled Fusion **59**, 055009 (2017).
[57]F. Nespoli, P. Tamain, N. Fedorczak, G. Ciraolo, D. Galassi, R. Tatali, E. Serre, Y. Marandet, H. Bufferand, and P. Ghendrih, "3D structure and dynamics of filaments in turbulence simulations of WEST diverted plasmas," Nucl. Fusion **59**, 096006 (2019).
[58]P. Paruta, C. Beadle, P. Ricci, and C. Theiler, "Blob velocity scaling in diverted tokamaks: A comparison between theory and simulation," Phys. Plasmas **26**, 032302 (2019).
[59]D. D'Ippolito, J. Myra, and S. Krasheninnikov, "Cross-field blob transport in tokamak scrape-off-layer plasmas," Phys. Plasmas **9**, 222–233 (2002).
[60]Y. Sarazin, P. Ghendrih, G. Attuel, C. Clément, X. Garbet, V. Grandgirard, M. Ottaviani, S. Benkadda, P. Beyer, N. Bian *et al.*, "Theoretical understanding of turbulent transport in the SOL," J. Nucl. Mater. **313–316**, 796–803 (2003).
[61]N. Bisai, A. Das, S. Deshpande, R. Jha, P. Kaw, A. Sen, and R. Singh, "Simulation of plasma transport by coherent structures in scrape-off-layer tokamak plasmas," Phys. Plasmas **11**, 4018–4024 (2004).
[62]N. Bisai, A. Das, S. Deshpande, R. Jha, P. Kaw, A. Sen, and R. Singh, "Edge and scrape-off layer tokamak plasma turbulence simulation using two-field fluid model," Phys. Plasmas **12**, 072520 (2005).
[63]M. Kočan, R. Pánek, J. Stöckel, M. Hron, J. Gunn, and R. Dejarnac, "Ion temperature measurements in the tokamak scrape-off layer," J. Nucl. Mater. **363–365**, 1436–1440 (2007).
[64]M. Kocan, F. Gennrich, A. Kendl, H. Müller, and A. U. Team, "Ion temperature fluctuations in the ASDEX upgrade scrape-off layer," Plasma Phys. Controlled Fusion **54**, 085009 (2012).
[65]O. E. Garcia, J. Horacek, R. Pitts, A. Nielsen, W. Fundamenski, J. Graves, V. Naulin, and J. J. Rasmussen, "Interchange turbulence in the TCV scrape-off layer," Plasma Phys. Controlled Fusion **48**, L1 (2005).
[66]D. Rudakov, J. Boedo, R. Moyer, P. C. Stangeby, J. Watkins, D. Whyte, L. Zeng, N. Brooks, R. Doerner, T. Evans *et al.*, "Far SOL transport and main wall plasma interaction in DIII-D," Nucl. Fusion **45**, 1589 (2005).
[67]J. Horacek, J. Adamek, H. Müller, J. Seidl, A. H. Nielsen, V. Rohde, F. Mehlmann, C. Ionita, E. Havlíčková *et al.*, "Interpretation of fast measurements of plasma potential, temperature and density in SOL of ASDEX upgrade," Nucl. Fusion **50**, 105001 (2010).
[68]R. Kube, O. E. Garcia, A. Theodorsen, D. Brunner, A. Kuang, B. LaBombard, and J. L. Terry, "Intermittent electron density and temperature fluctuations and associated fluxes in the alcator C-Mod scrape-off layer," Plasma Phys. Controlled Fusion **60**, 065002 (2018).
[69]B. Dudson, M. Umansky, X. Xu, P. Snyder, and H. Wilson, "BOUT++: A framework for parallel plasma fluid simulations," Comput. Phys. Commun. **180**, 1467–1480 (2009).
[70]B. Dudson, P. Hill, D. Dickinson, J. Parker, A. Allen, G. Breyiannia, J. Brown, L. Easy, S. Farley, B. Friedman, E. Grinaker, O. Izacard, I. Joseph, M. Kim, M. Leconte, J. Leddy, M. Løiten, C. Ma, J. Madsen, D. Meyerson, P. Naylor, S. Myers, J. Omotani, T. Rhee, J. Sauppe, K. Savage, H. Seto, D. Schwörer, B. Shanahan, M. Thomas, S. Tiwari, M. Umansky, N. Walkden, L. Wang, Z. Wang, P. Xi, T. Xia, X. Xu, H. Zhang, A. Bokshi, H. Muhammed, and M. Estarellas (2019). BOUT++ v4.3.0 (Version 4.3.0). Zenodo. http://doi.org/10.5281/zenodo.3518905
[71]G. D. Byrne and A. C. Hindmarsh, "PVODE, an ODE solver for parallel computers," Int. J. High Perform. Comput. Appl. **13**, 354–365 (1999).
[72]S. Hoyer and J. Hamman, "xarray: ND labeled arrays and datasets in python," J. Open Res. Software **5**, 10 (2017).
[73]O. E. Garcia, R. Kube, A. Theodorsen, and H. Pécseli, "Stochastic modelling of intermittent fluctuations in the scrape-off layer: Correlations, distributions, level crossings, and moment estimation," Phys. Plasmas **23**, 052308 (2016).
[74]R. Kube, O. E. Garcia, A. Theodorsen, A. Kuang, B. LaBombard, J. L. Terry, and D. Brunner, "Statistical properties of the plasma fluctuations and turbulent cross-field fluxes in the outboard mid-plane scrape-off layer of alcator C-Mod," Nucl. Mater. Energy **18**, 193–200 (2019).
[75]A. Theodorsen, O. E. Garcia, J. Horacek, R. Kube, and R. Pitts, "Scrape-off layer turbulence in TCV: Evidence in support of stochastic modelling," Plasma Phys. Controlled Fusion **58**, 044006 (2016).
[76]O. E. Garcia, R. Kube, A. Theodorsen, J.-G. Bak, S.-H. Hong, H.-S. Kim, and R. Pitts, "Sol width and intermittent fluctuations in KSTAR," Nucl. Mater. Energy **12**, 36–43 (2017).
[77]G. Decristoforo and T. Nicholas, "xblobs v1.0.0," (2020). Zenodo. http://doi.org/10.5281/zenodo.4091041